A POWER DENSE DC-DC CONVERTER FOR A SMALL ELECTRIC VEHICLE

F.J. Bryan*, A.J. Forsyth*

*University of Manchester,UK. F.Bryan@manchester.ac.uk

Abstract

A power dense DC-DC converter is required to interface a supercapacitor energy buffer with a higher voltage traction drive in a small electric vehicle application. A converter design and component selection process is described for a bidirectional, 18 kW, dual interleaved boost converter with interphase transformer. The physical construction of the converter is optimised to increase volumetric and gravimetric power density and simplify assembly. The prototype converter achieves a power density of 6.5 kW/kg and 7.9 kW/l. Converter efficiency and thermal results are presented and component mass and loss audits are included.

1 Introduction

Electric vehicle traction drives are often operated at fixed high voltages to improve traction system efficiencies whilst sources such as supercapacitors, batteries and fuel cells often operate at lower voltages, which vary with demand or state-of-charge. DC-DC converters are therefore required to interface these components with, high power density being a key design criterion of automotive systems.

The target vehicle in this research was a small electric vehicle (1800 kg) which utilises a 200 V, 20 kW, traction drive, a 10 kW fuel cell with voltage varying from 140 V to 70 V at full load and a supercapacitor bank operating between 100 V and 50 V. The drive-train configuration is shown in Figure 1 and the 18 kW bidirectional converter used to interface the supercapacitors is the focus of this paper.
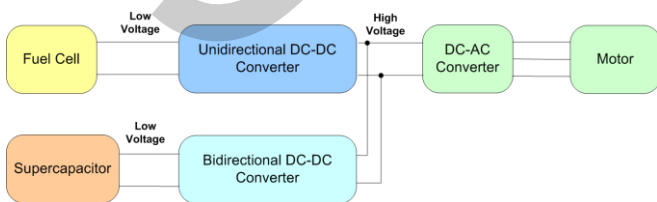

Figure 1. Traction System Architecture

2 Converter Topology

The boost converter is a simple non-isolated topology, which has been widely implemented in vehicles due to its simplicity [1-5]. The drawback of the converter is the discontinuous output current resulting in a larger capacitor requirement. The majority of designs therefore operate multiple converters in parallel with an 'interleaved' switching pattern. A variation of this approach is used by Calderon-Lopez [1] and Hirakawa [6] where a single inductor is used along with an interphase transformer (IPT) or inversely coupled inductor shown in Figure 2.
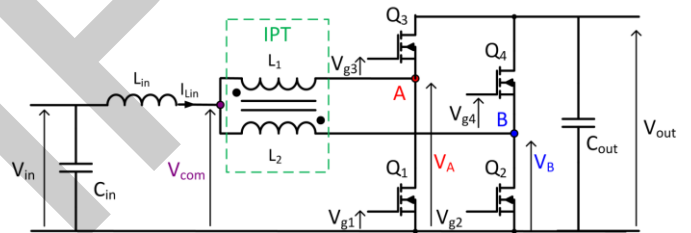

Figure 2. Interleaved Boost Converter with IPT

The interleaved boost converter with IPT switches with a phase shift of 180 ° and uses the IPT to reduce the AC voltage across the input inductor. Furthermore, the input inductor is subjected to operation at twice the switching frequency, reducing the inductance requirement for a given input current ripple and allowing the use of smaller magnetic cores. A cancellation of the DC flux is also experienced by the IPT allowing its design to be optimised for AC excitation. A range of designs for an IPT configuration and a two inductor configuration are compared in [1] and the IPT designs result in consistently lower losses. The IPT circuit is therefore likely to produce lower losses and lower mass magnetic components which should result in a higher power density converter.

Assuming that the input current is shared equally by the two phases and that the input current is continuous, three distinct operating modes are possible for Duty ratio D: D < 0.5, D = 0.5 and D > 0.5. Figure 3 shows the operation of the converter using ideal, lossless components, at D = 0.5 and D = 0.75, the two extremes of operation for this converter.
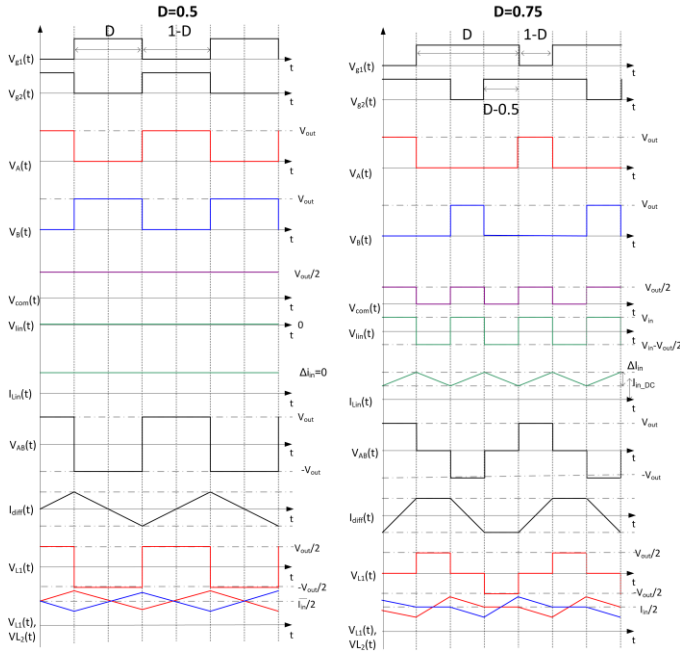
Figure 3. Dual interleaved boost with IPT waveforms

3 Converter Design and Construction

Water cooling is used as a common method of reducing the volume of a converter as the internal space required for air flow is no longer required. The thermal management concept for the converter is to use a single liquid-cooled cold plate to remove all losses, allowing the final unit to be housed in a sealed case. It is assumed that the converter is a minimum of 95 % efficient at maximum input power resulting in 900 W of losses when operating at 18 kW. The Lytron CP15 [7] pressed tube aluminium cold plate is used as a typical off-the-shelf water-cooled cold plate. The CP15 has a thermal resistance of 0.01 ˚C/W resulting in a cold plate surface temperature of 64 ˚C assuming the coolant temperature is 55 ˚C, the maximum coolant temperature for the traction drive in this example.

3.1 MOSFETS

The switching device losses are calculated for operation in boost mode as in this application there is a higher demand during vehicle acceleration than during supercapacitor recharge. In this operating mode, Q_1 and Q_2 are the conducting MOSFETs whilst the body diodes of MOSFETs Q_3 and Q_4 are operated as the converter freewheeling diodes.

It is assumed that the currents in the converter are shared equally by the two phases due to the use of peak current mode control and the losses in the devices are therefore considered to be equal for each leg, $P_{Q1} = P_{Q2}$ and $P_{Q3} = P_{Q4}$.

A range of 300 V, 100-140 A, MOSFETS were compared and the APT30M17JLL device was selected due to lower expected losses and a low junction to heat-sink thermal resistance.

3.2 Inductor

To design the inductor an algorithm was used to identify inductor designs which satisfy the minimum inductance requirement for the converter specification. A range of core parameters is loaded, in this case the FINEMET C core range from Hitachi are used due to the low loss and high operating flux limit (1.2 T). For each core size, the gap length is calculated for an increasing number of turns from one to an upper limit. Designs which have a gap length, which exceeds the manufactures recommendations are removed from the suitable designs list. The peak flux density is then calculated to ensure it does not exceed the material saturation point. The gap, core and copper losses are then calculated using equations from [8, 9] assuming a copper foil winding. There are multiple solutions that satisfy the converter requirement, for each core, trading the gap length against an increasing number of turns. The results allow a comparison of suitable designs by individual loss mechanisms as well as total component loss.

Equation (1), from [8, 10], describes the required air-gap, l_g, to satisfy a given inductance requirement, L, assuming a peak current, $\hat{I}$, maximum flux, B_{MAX}, and a core cross-sectional area, A_c.

$$l_g = \frac{4\pi\left(10^{-7}\right)N^2 F A_C}{L} \tag{1}$$

The fringing flux at the core gap has the effect of reducing the reluctance of the circuit and therefore increasing the inductance, L. Equation (2) from [8] is an approximation of the fringing factor, F, to account for this effect, where c is the core window height.

$$F = 1 + \left(\frac{l_g}{\sqrt{A_C}}\right)\ln\left(\frac{2c}{l_g}\right) \tag{2}$$

To remove the recursive process for calculating the fringing factor, equations (1) and (2) are combined to form (3) which can be rearranged into the form of (4) where p is defined by (5).

$$l_g = \left(\frac{4\pi\left(10^{-7}\right)N^2 A_c}{L}\right)\left(1+\left(\frac{l_g}{\sqrt{A_C}}\right)\ln\left(\frac{2c}{l_g}\right)\right) \tag{3}$$

$$\frac{p\sqrt{A_C}}{2c}e^{\sqrt{A_C}} = \frac{p\sqrt{A_C}}{l_g}e^{\frac{p\sqrt{A_C}}{l_g}} \tag{4}$$

$$p = \frac{4\pi(10^{-7})N^2 A_c}{L} \tag{5}$$

The Lambert function, denoted by the operator W, can be used to calculate the solution of equation (6) for any complex

number, z. This allows equation (4) to be resolved into equation (7).

$$z = W(z)\,e^{W(z)} \qquad (6)$$

$$l_g = \frac{\sqrt{A_C}}{W\left(\dfrac{\sqrt{A_C}}{2c}\,e^{\dfrac{L\sqrt{A_C}}{4\pi\left(10^{-7}\right)N^2 A_C}}\right)} \qquad (7)$$

The approximated losses of the most efficient design for each core are shown in Figure 4. The inductor designs are then compared using a thermal FEA model to approximate the temperature rise in the hotspot of the core. This allows the smallest core design to be selected that does not exceed the thermal limit of the core epoxy including a safety factor.
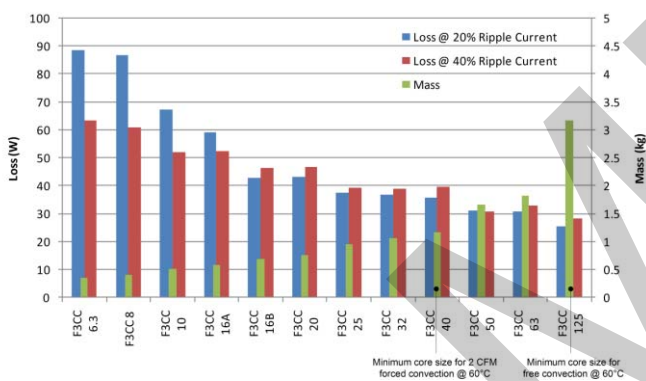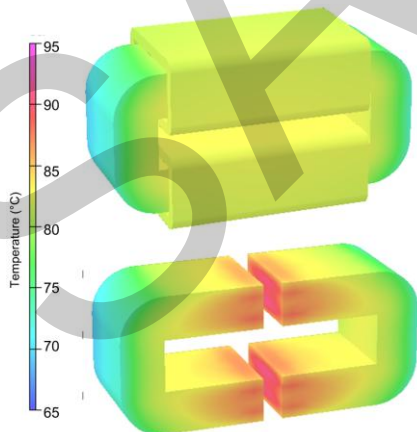

Figure 4. Inductor Loss Comparison

Figure 5. Inductor thermal FEA model example result

The FEA model has been experimentally validated and produced less than a 5°C error in experimental testing [9]. The model assumes the inductor is encased in an aluminium heat-sink as shown in Figure 6. The simulation results identify the F3CC0025 core as a thermally suitable design, which is smaller than the F3CC0040 core selected for forced air cooling at 2 CFM.
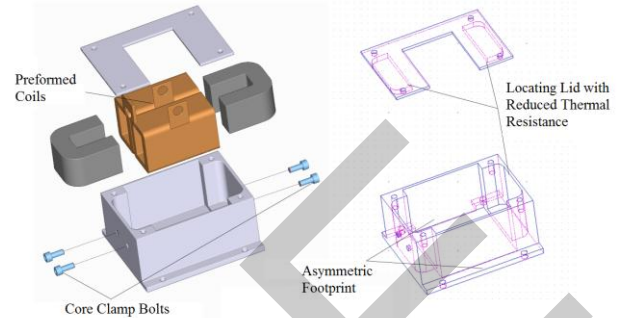

Figure 6. Potted inductor drawing

3.3 Interphase Transformer

The IPT design is performed in the same manner as the inductor design, but the highest losses occur at 50 % duty ratio, with maximum input current, 180 A, since under this condition the V_A-V_B voltage is a square-wave of $\pm V_{out}$, resulting in the maximum AC flux condition. As the IPT has very little DC flux it is not gapped and so the losses are more evenly distributed throughout the core and coil. This is apparent in the example IPT FEA results shown in Figure 7 for a ferrite ETD core and FINEMET C core, left and right respectively, compared with the inductor results in Figure 5.
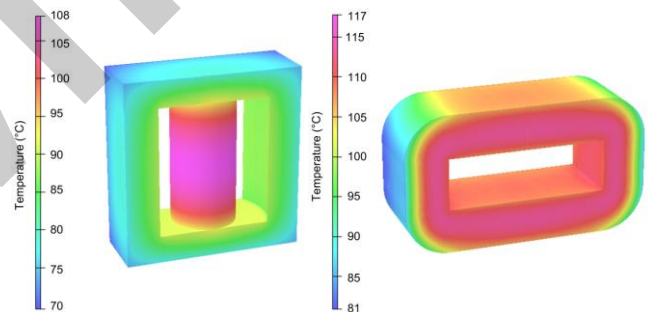

Figure 7. IPT thermal FEA model example results

3.4 Bus-bars and Capacitors

The bus-bars are etched copper sheets. A large surface is used and a thin layer of insulation to reduce EMI from the bus-bars and to minimise parasitic inductance [11]. Adhesive polyimide 'Kapton' tape is applied to the copper sheets before assembly. The bus-bars are etched to locate onto a number of nylon pillars mounted on the cold plate. The bus-bars are then connected directly to the switching devices using aluminium pillars to simplify assembly and reduce converter height.

The EVS ceramic capacitor series was selected as these components have a lower mass and volume than the alternative polypropylene capacitors. The ceramic capacitors have only 8 % of the volume of the Colonel Dubilier polypropylene alternative, with the added advantage of the

low profile package improving heat extraction [12]. These capacitors also appear to have been an enabling feature of the power dense converter described by Hirakawa [6].
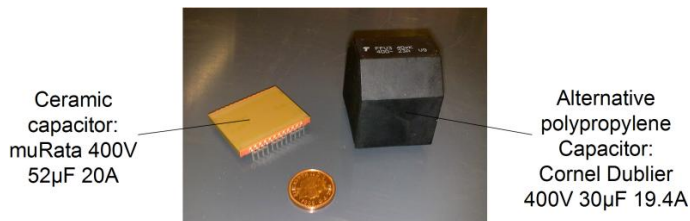

Figure 8. Capacitor comparison

The converter uses a double-sided connection of capacitors on the bus-bar before the module is mounted onto the converter. This reduces the converter footprint and ensures equal distances between all of the capacitors to improve current sharing.
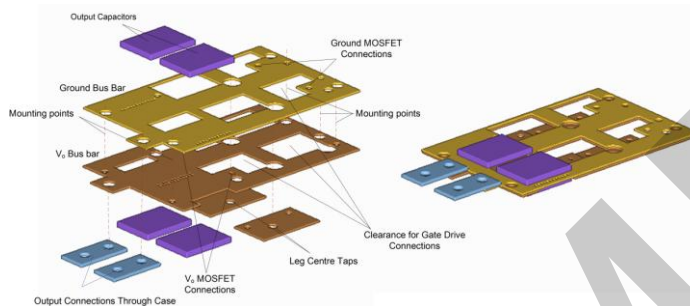

Figure 9. Bus-bar and capacitor module

3.5 Physical construction

The converter is constructed around a pressed copper tube aluminium water-cooled cold-plate. The cold-plate acts as the central structure of the converter, the switching devices and output capacitors are on the top face and the two potted magnetic components are on the bottom to maximise utilisation of the cooling surfaces.

The inductor and IPT are encased in aluminium heat-sinks with a small clearance around the components filled with a thermally conductive compound. The inductor is a FINEMET C core (F3CC0025), wound with copper foil whilst the IPT is an Epcos ETD59 core wound with strands of enamelled copper wire. The inductor and IPT are shown before potting in their aluminium enclosures in Figure 10 from left to right respectively.
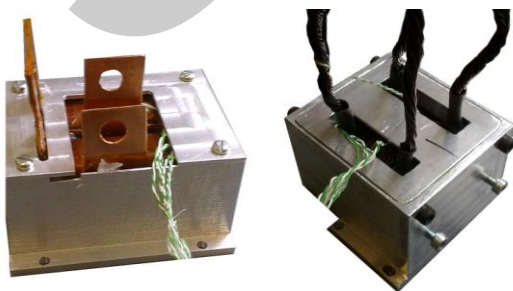

Figure 10. Magnetic components in aluminium heat-sinks

Figure 11 shows the exploded converter diagram identifying the key components whilst Figure 12 is a photograph of the prototype converter.
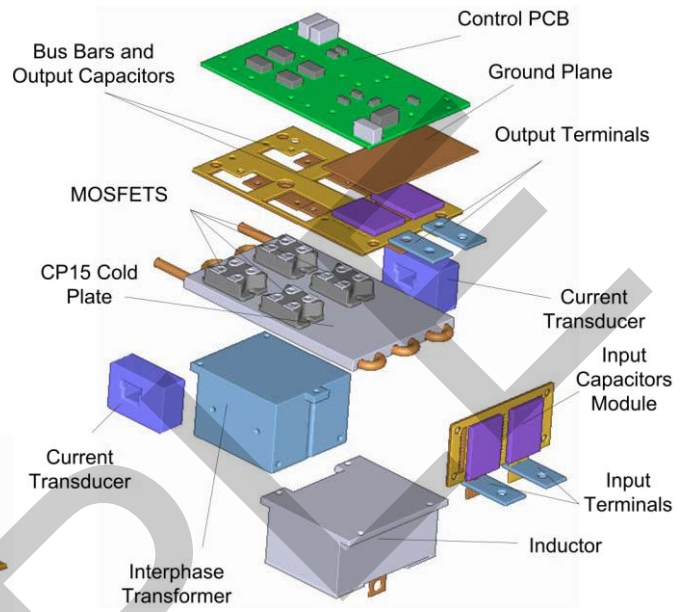
Figure 11. Converter exploded diagram
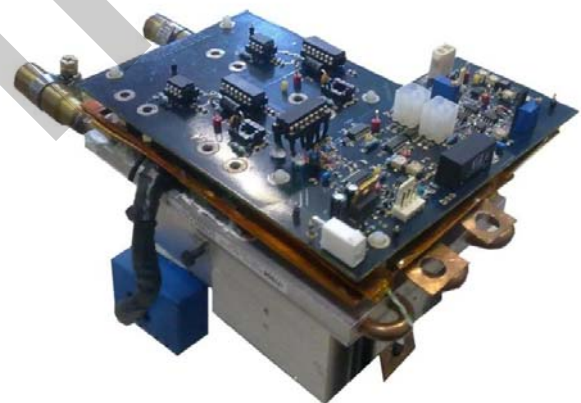
Figure 12. Converter prototype

The converter prototype shown in Figure 12 achieves 18 kW operation in a volume of 2.3 litres resulting in a power density of 7.8 kW/l. The masses of the individual components are shown in Table 1, including an approximated casing mass assuming a 1.5 mm thick aluminium enclosure. The total uncased mass is 2.79 kg resulting in a gravimetric power density of 6.45 kW/kg, this is reduced to 4.3 kW/kg when the casing is included as the total mass is increased by 49 %.

Table 1. Converter mass breakdown

Component	Description	Mass (g)
Copper bus-bars	Input and output copper bus-bars	122
Filter capacitors	Murata filter capacitors Input and output	208
MOSFETs	Switching devices	116
Cold plate	Lytron CP15 cold plate (dry)	348
Inductor and coil	F3CC0025 FINEMET core and copper coil	660
Inductor casing	Potting compound and aluminium for inductor	396
IPT core and coil	ETD59 core and copper coil	544
IPT casing	Potting compound and aluminium for IPT	293
PCB	PCB populated with components	81
Mounting pillars etc.	Mounting pillars, cabling, connectors	100
Casing	Predicted mass of a 1.5mm aluminium case surrounding the converter volume +10% for mounting	1360
TOTAL	Total converter mass (including case)	2787 (4147)

4 Converter Test Results and Losses

The converter efficiency was measured at a range of input voltages and powers and compared with the loss approximations used in the design. At low current operation the converter operates at approximately 98% efficiency. As the converter power is increased the efficiency drops as low as 90 %.

The expected efficiency at minimum input voltage, 50 V, is within 1 % of the measured efficiency. The expected losses in the converter are dominated by the conduction losses in the MOSFETs and small errors can be accounted for by an increased device resistance over the specified value. The approximations of the IPT and inductor losses will have a smaller effect as the combined magnetic component losses account for approximately one sixth of the total converter losses.

At the maximum input voltage, 100 V, the difference is significantly greater between expected and measured efficiency values. At powers below 15 kW the trend is towards a peak power efficiency of 94 %, similar to the expected value. Table 2 shows a breakdown of approximated losses and the converter efficiency at maximum input voltage (50 % duty ratio) and minimum input voltage (75 % duty ratio).

Table 2, Estimated major component losses

Duty Ratio	Inductor	IPT	Each MOSFET	Each Diode	Efficiency (Power)
50 %	23 W	68 W	180 W	55 W	96 % (18 kW)
75 %	39 W	45 W	272 W	28 W	92 % (9)kW

The temperature rise of a number of thermocouples embedded in the inductor and IPT is shown in Tables 3 and 4 for operation at 75 % duty ratio and 50 % duty ratio respectively. The results are within 5 °C of the FEA model steady state predictions.

Table 3. Steady state temperature rise over heat-sink at 50% duty ratio, 175A input current

Location	Temperature rise above heat-sink
Inductor gap face 1	3 °C
Inductor gap face 2	3 °C
Inductor core side	3 °C
IPT core centre	40 °C
IPT coil centre	29 °C
IPT coil top	28 °C
IPT core mid leg	20 °C

Table 4. Steady state temperature rise over heat-sink at 75% duty ratio, 160A input current

Location	Temperature rise above heat-sink
Inductor gap face 1	24 °C
Inductor gap face 2	25 °C
Inductor core side	6 °C
IPT core centre	42 °C
IPT coil centre	33 °C
IPT coil top	32 °C
IPT core mid leg	7 °C

The model accuracy is higher for the inductor than for the IPT as the individual strands copper winding are more complex to model due to the increased number of thermal boundaries.

5 Conclusions

A prototype DC-DC converter has been designed and constructed to achieve a high power density, 7.8 kW/l and 6.45 kW/kg. The converter uses a water cooled cold-plate and magnetic components potted in aluminium heat-sinks to achieve the power density. An inductor design algorithm for comparing losses and a thermal FEA model of the magnetic components has been used to identify a low volume and low mass solution within material thermal limits.

References

[1]   G. Calderon-Lopez, A. Forsyth, and D. R. Nuttall, "Design and Performance Evaluation of a 10-kW Interleaved Boost Converter for a Fuel Cell Electric Vehicle," in *Power Electronics and Motion Control Conference*. vol. 2, 2006.

[2]   M. Gerber, J. A. Ferreira, I. W. Hofsajer, and N. Seliger, "A very high density, heatsink mounted inductor for automotive applications," in *Industry Applications Conference, 2002. 37th IAS Annual Meeting. Conference Record of the*, 2002, pp. 948-954 vol.2.

[3]   M. Gerber, J. A. Ferreira, N. Seliger, and I. W. Hofsajer, "Design and evaluation of an automotive integrated system module," in *Industry Applications Conference, 2005. Fourtieth IAS Annual Meeting. Conference Record of the 2005*, 2005, pp. 1144-1151 Vol. 2.

[4]   M. Gerber, J. A. Ferreira, N. Seliger, and I. W. Hofsajer, "Integral 3-D thermal, electrical and mechanical design of an automotive DC/DC converter," *Power Electronics, IEEE Transactions on,* vol. 20, pp. 566-575, 2005.

[5]   B. Eckardt, A. Hofmann, S. Zeltner, and M. März, "Automotive Powertrain DC/DC Converter with 25 kW/dm3 by using SiC Diodes," 2006, pp. 7–9.

[6]   M. Hirakawa, M. Nagano, Y. Watanabe, K. Andoh, S. Nakatomi, and S. Hashino, "High power density DC/DC converter using the close-coupled inductors," in *Energy Conversion Congress and Exposition, 2009. ECCE 2009. IEEE*, 2009, pp. 1760-1767.

[7]   Lytron Inc,"cold_plate_techcomp_chart", 2008, available online from: www.lytron.com/cold-plates/cold-plates-overview.aspx [04/05/10]

[8]   W. T. McLyman, *Magnetic Core Selection for Transformers and Inductors*. New York: Marcel Dekker, 1982.

[9]   F. Bryan, "Power Train Design for Small Fuel Cell Vehicles" University of Manchester, Manchester, EngD Thesis, Jan 2011

[10]   Metglas Inc,"Application Guide: Power Factor Correction Inductor Design For Switched Mode Power Supplies Using Metglas Powerlite C-Cores", 2009, available online from: http://www.metglas.com/downloads/apps/pfc.pdf [08/08/10]

[11]   M. C. Caponet, F. Profumo, R. W. De Doncker, and A. Tenconi, "Low stray inductance bus bar design and construction for good EMC performance in power electronic circuits," in *Power Electronics Specialists Conference, 2000. PESC 00. 2000 IEEE 31st Annual*, 2000, pp. 916-921 vol.2.

[12]   T. Kageyama,"Murata's Ceramic Capacitor Serves Next Series of Power Electronics", 2007, available online from: http://www.murata.com/articles/ta06d2.pdf [01/10/2010]